Stress and temperature dependence of screw dislocation mobility in bcc-Fe by molecular dynamics

J. Marian, S. Queyreau, M. Gilbert

March 29, 2011

Disclaimer

This document was prepared as an account of work sponsored by an agency of the United States government. Neither the United States government nor Lawrence Livermore National Security, LLC, nor any of their employees makes any warranty, expressed or implied, or assumes any legal liability or responsibility for the accuracy, completeness, or usefulness of any information, apparatus, product, or process disclosed, or represents that its use would not infringe privately owned rights. Reference herein to any specific commercial product, process, or service by trade name, trademark, manufacturer, or otherwise does not necessarily constitute or imply its endorsement, recommendation, or favoring by the United States government or Lawrence Livermore National Security, LLC. The views and opinions of authors expressed herein do not necessarily state or reflect those of the United States government or Lawrence Livermore National Security, LLC, and shall not be used for advertising or product endorsement purposes.

Stress and temperature dependence of screw dislocation mobility in α-Fe by molecular dynamics.

Mark R. Gilbert[a], Sylvain Queyreau[b], and Jaime Marian[b]

[a]*EURATOM/CCFE Fusion Association, Culham Science Centre, Abingdon, Oxon, OX14 3DB, UK*
[b]*Lawrence Livermore National Laboratory, Livermore, CA 94551*

Abstract

We have performed molecular dynamics simulations of $\frac{1}{2}\langle 111\rangle\{112\}$ screw dislocation motion as a function of temperature and stress to obtain mobility relations suitable for mesoscale computational techniques. We find two dynamic regimes governed by different mechanisms of motion. Consistent with experimental evidence, at low stresses and temperatures the dislocations move by thermally activated nucleation and propagation of kink pairs. At a critical stress, a temperature dependent transition to a viscous linear regime is observed. Critical output from the simulations, such as threshold stresses and the stress dependence of the kink activation energy, are compared to experimental data and other atomistic works with generally very good agreement. Additionally, we find that the viscous drag coefficient is nearly temperature independent. Contrary to some experimental interpretations, we find that glide on $\{112\}$ planes is only apparent, as slip always occurs by elementary kink pair nucleation/propagation events on $\{110\}$ planes. This is mediated by a dislocation core transformation from compact to dissociated identified above room temperature. We discuss the relevance and applicability of our results and provide a closed-form functional mobility law based on physical behavior extracted from the MD simulations.

Keywords: Screw dislocations, Fe plastic behavior, dislocation mobility, molecular dynamics

1. Introduction

The low temperature yield behavior of α-Fe single crystals has been well characterized over the years in numerous experimental works [1, 2, 3, 4]. Tensile tests in high-purity specimens reveal a strongly temperature-dependent strain rate behavior and flow stress [5, 6]. This is known to be a consequence of the thermally-activated nature of $\frac{1}{2}\langle 111\rangle$ screw dislocation motion in body-centered cubic (bcc) metals. Because lattice friction in such crystals is typically quite high, at moderate to low stresses, plastic flow can be reduced to the individual motion of screw dislocations, which are known to display much lower mobilities than non-screw dislocations. Consequently, by studying single screw dislocation properties and mobilities, many useful insights can be gained into the plastic behavior of Fe and other bcc crystals.

However, experimental measurements concerning single dislocation properties are exceedingly difficult, and only recently have experimental techniques reached a level of resolution capable of isolating individual dislocation behavior [7, 8], particularly in bcc Fe [9]. Consequently, a wealth of atomistic simulation studies have been performed over the last decade or so in an attempt to shed light on dislocation structure and core properties and energetics [10, 11, 12, 13, 14]. In particular, the stress dependence of the kink-pair (KP) nucleation enthalpy has been the subject of much study [15, 16, 17, 18]. Nevertheless,

despite these and other significant advances in our understanding of $\frac{1}{2}\langle 111\rangle$ screw dislocation properties at the atomistic level, their true impact on plasticity on a more global scale can only be assessed by way of models operating at the mesoscale, *e.g.* dislocation dynamics or phase fields. Indeed, screw dislocation-controlled plasticity in α-Fe has been the subject of several dislocation dynamics (DD) works [19, 20]. The fundamental input to DD simulations is the so-called mobility function [21, 22, 23], which couples forces acting on dislocation segments to their velocity response. On a more simplistic level, the mobility function relates applied stresses to dislocation velocities, and may be a function of several factors, including temperature, pressure, dislocation character, and internal microstructure.

In extracting this information directly from experimental observations it is typically exceedingly difficult to subtract out the effect on mobility of the surrounding dislocation environment, although notable exceptions exist [9]. Conversely, if used carefully, atomistic simulations can be invaluable in providing dislocation mobility behavior under well-controlled conditions [24, 25]. In this paper we present a molecular dynamics (MD) study of $\frac{1}{2}\langle 111\rangle$ screw dislocation motion in bcc Fe as a function of stress and temperature. At low temperatures, screw dislocations are known to move as straight lines, which suggests that only one KP exists at a given time. This is the basis of the so-called *smooth* glide identified in ref. [26]. Such a regime is then governed by KP nucleation, as kink motion proceeds at comparatively high speeds. These are precisely the conditions for which we have designed our simulations, as will be shown below. However, this is no longer the case at higher temperatures, where kink nucleation and propagation can be of the same order of magnitude. This is the prelude to the famed phonon drag regime that sets in when kink nucleation is no longer the rate limiting step.

This paper is organized as follows, first we perform a careful study of the simulation geometry. Second, we present the MD data and provide the theoretical framework to justify the fitting functions used to produce analytical mobility laws. This is followed by an analysis of the proposed mobilities and the implications for crystal plasticity. Our calculations are performed with the parallel MD code LAMMPS [27] using the EAM potential for Fe developed by Mendelev *et al.* [28]. The literature on screw dislocation core properties [29, 13, 30, 14], Peierls energy and stress [14, 31], kink structure and formation energies [30, 17, 31, 18], to name but a few, using this potential is quite abundant, and here we simply note that this potential yields the symmetric core structure (at 0K) predicted by electronic structure calculations [13, 14, 32].

2. Methodology

Dislocation mobility calculations require long simulation times to allow for a steady state to be reached under each set of conditions. This means that setups such as those employed by Domain and Monnet [13] or Chaussidon *et al.* [30], which result in finite dimensions along the glide direction (referred to by the authors as 'free boundaries'), cannot be used here. Instead, we use periodic boundary conditions along the dislocation line and glide directions, and traction boundaries along the glide plane normal direction. This imposes certain restrictions on the computational box dimensions L_x, L_y, and L_z, each one governed by a specific physical process. Next, we discuss the criteria chosen for the design of each dimension of the supercell on the basis of the relevant physical phenomena.

2.1. Line direction.

At low temperatures and stresses, $\frac{1}{2}\langle 111\rangle$ screw dislocations move by nucleation/propagation of kink pairs. These KPs display a stress and temperature dependent characteristic separation length that must be contained entirely within the dislocation line. Marian *et al.* [26] showed that short dislocation segments result in 2D dynamics, not representative of dislocation motion at low *T*. In addition, recent work by Ventelon *et al.* [17] suggests that single kinks in Fe have widths of the order of 20*b* in the $\langle 111\rangle$ direction at 0K. Despite the fact that the calculations by Ventelon *et al.* concern only single, isolated kinks, and thus neglect the interaction between the two kinks of a KP, which could indeed alter this value, here we use a lower bound length of 40*b* for our screw dislocation lines, where $b = a_0\frac{\sqrt{3}}{2} \approx 0.25$ nm is the Burgers vector and $a_0 = 0.27$ nm is the lattice parameter for bcc Fe.

An upper bound is obtained by considering the conditions under which the KP mechanism results in linear, smooth glide as defined in Ref. [26][†]. As shown there, when the dislocation line is too long, the simulation limitations inherent to MD result in multiple kinks on multiple glide planes, leading to cross kinks. This so-called *rough* regime results in self-pinning and is not representative of plasticity at moderate to low stresses and temperatures. Following the arguments provided by Marian *et al.* [26], ensuring that only one KP occurs simultaneously requires that the kink mean-free-path *X* be at least as large as the dislocation length *L*. *X* is defined as:

$$X = 2\sqrt{\frac{v_k}{J_k}} \tag{1}$$

where v_k is the kink velocity and J_k is the KP nucleation rate:

$$J_k = \frac{v_k}{a^2}\exp\left(-\frac{H_{\text{KP}}(\sigma)}{kT}\right), \tag{2}$$

where *a* is the average kink separation distance within the KP and $H_{\text{KP}}(\sigma)$ is the formation enthalpy of a KP at a stress σ. Equating *X* to *L* yields:

$$L = a\exp\left(\frac{H_{\text{KP}}(\sigma)}{2kT}\right)$$

For $H_{\text{KP}}(\sigma)$ one can use the phenomenological expression due to Kocks, Argon and Ashby [33]:

$$H_{\text{KP}}(\sigma) = H_0\left(1 - \left(\frac{\sigma}{\sigma_P}\right)^p\right)^q \tag{3}$$

where H_0 is the KP formation enthalpy at zero temperature and stress, σ_P is the Peierls stress, and *p* and *q* are fitting parameters. Using H_0=0.65 eV [14], τ_P=1200 MPa [30], and the values predicted by linear elasticity *p*=0.5 and *q*=1.25, one can use the values of *a* at different stresses calculated by Ngan *et al.* [34] with which to estimate *L* from eq. 3. On the basis of these simulations we found a value of $L_y = 80b \approx 19.8$ nm to be sufficient for the temperature and stress ranges of interest in this work.

[†]Also termed the 'single kink-pair' regime by Chaussidon *et al.* [30].

2.2. Plane normal direction

In the conventional picture of α-Fe plasticity, supported by a myriad of experimental studies (cf. 1), slip takes place on {110} planes across the entire temperature range when they are the most highly stressed planes. However, for the potential employed here, this maximum resolved shear stress (MRSS) plane is also the glide plane only in a narrow range of (low) temperature and stress. Indeed, Domain and Monnet [13] and Chaussidon *et al.* [30] have shown that consistent {110} slip is only attainable under dynamic conditions when free boundaries are used along the glide direction. As pointed out above, these boundary conditions are not suitable for the type of dislocation mobility calculations that we are concerned with here. As the applied stress and simulation temperature increase, screw dislocations are seen to deviate from {110} planes and rotate to glide planes that approach {112}. MD simulations have confirmed that despite gliding on *effective* {112} planes, slip proceeds as a succession of elementary kink nucleation episodes on non-MRSS {110} planes [26, 30].

Therefore, here we have chosen to study dislocation motion on {112} planes, with stress applied to a skin layer consisting of three atomic planes at the top and bottom of the simulation box. These layers can relax in-plane but are fixed along the z-direction (glide plane normal). Although these boundary conditions are known to introduce non-glide stresses [30], they provide repulsive image forces [35], which result in stable glide conditions. Temperature control is also only applied to atoms in the skin region via a Langevin thermostat. Once the dislocated crystallites have been generated at the desired temperature, stress-controlled simulations are performed without any kind of temperature control in the bulk region of the computational box.

The dimension along the $\langle 112 \rangle$ direction is obtained on the basis of the following arguments:

(i) When stress is initially applied, a shear stress wave traveling at the speed of sound is generated at each of the skin layers. These waves cross the sample and reflect off the opposite boundaries with inverted sign, which cancels the effect of fresh stress waves coming from the surface. This makes the dislocation stop until these elastic waves reverberate again at the original boundary and restore their sign. This process repeats itself until the waves are suppressed by viscous damping and scattering. As we shall see (*e.g.* cf. Fig. 3), this results in a transient period during which dislocation mobility is highly scale dependent. With L_z too small, every reflection is only dampened very slightly, which could then cause the movement of dislocations to be too intermittent for a steady state to be reached within reasonable MD time scales.

(ii) As we have indicated above, the rigid boundaries where the stress is applied, create repulsive forces on the dislocation that stabilize it on the glide plane corresponding to the center of the box. However, because the presumed mechanism of motion on MRSS {112} glide planes is still by complementary KP nucleations on the {110} planes bordering at $\pm 30°$, the image forces must be sufficiently small to not interfere with this natural mechanism. This suggests a z dimension as large as possible.

On the basis of these considerations, a reasonable size was found to be 58.7 nm or $L_z = 84\sqrt{6}a_0$. Stress was always applied so as to create a Peach-Köhler force in the twinning sense.

2.3. Glide direction

The physical consideration to keep in mind when designing the dimension L_x along the periodic glide direction $\langle 110 \rangle$ is local heating after each dislocation passage. Fast-moving dislocations leave a 'hot' trail

in their wake in the regime governed by viscous drag. In contrast to dislocations moving in an *effective* infinite medium, which see only a 'fresh' crystal ahead, in MD simulations the dislocation re-enters the box after each passage (we emphasize again that single-passage simulations are not acceptable for our dynamic mobility simulations). The residual heat remaining locally on the glide plane dissipates at a given rate that depends on temperature, material properties, and dissipation direction. If the dislocation encounters a hot glide plane after each passage the resulting velocity would not be representative of the simulation temperature, and, thus, the computational box must be sufficiently large in the glide direction to ensure that the dislocation travels through a thermalized glide plane on every passage.
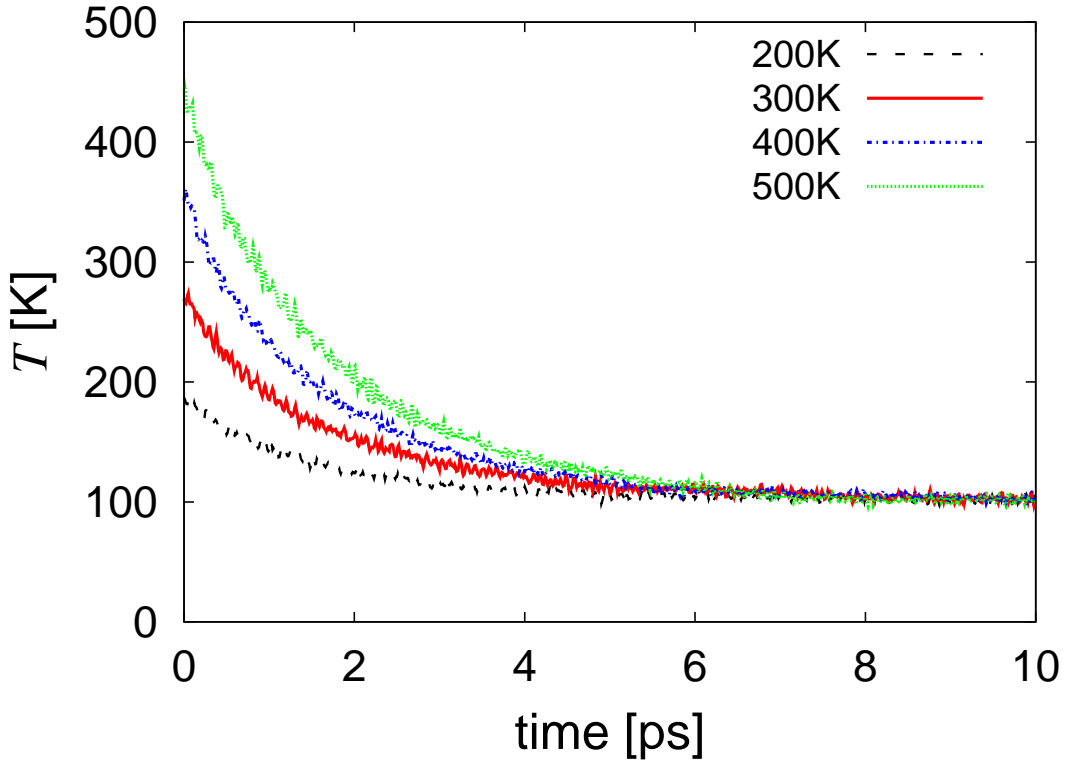

Figure 1: Evolution of the initial temperature in a computational cell after connecting the skin region to a heat reservoir at 100K. For all the initial temperatures, a decay time constant of ≈ 7 ps is found.

To obtain a first order estimate of L_x, we set up a small $10 \times 10 \times 10 a_0$ box in which a central region of atoms was initialized at different temperatures greater than 100K and a skin region was kept at a constant temperature of 100K. The temperature decay profile of the central region was then fitted to the inverse exponential solution to Newton's law of cooling:

$$T(t) = T_\infty + a \exp(-bt),$$

where, in the simulations, T_∞ is the final target temperature, a and b are fitting constants that represent, respectively, the initial temperature difference between the central atoms and the skin region at T^∞, and the decay constant. We are particularly interested in the latter, as it gives an idea of how fast heat is evacuated from atoms that are not subjected to temperature control. For the tests performed in Fig. 1

5

with $T^\infty = 100$K, we obtain an average value of $b \approx 0.55$ ps^{-1}, corresponding to a time constant of 1.8 ps. As the figure shows, at $t \approx 7$ ps all the curves have decayed to the temperature of the heat bath. Then, assuming a maximum dislocation velocity equal to the shear wave velocity of $\approx$3400 m·s^{-1} in Fe [28], the minimum box size along the glide direction is approximately 24 nm. Therefore we choose a box with $L_x = 60\sqrt{2}a_0 = 24.3$ nm. Before performing dislocation mobility simulations under applied stress, the box is equilibrated at the desired temperature during 20 ps using a Langevin thermostat. After applying stress, the total box temperature was never seen to increase more than 10% above the temperature of the heat bath.

Thus, to summarize this section, we have designed an orthogonal computational box with axes $z \equiv \frac{1}{2}[111]$, $y \equiv [11\bar{2}]$, and $x \equiv [\bar{1}10]$ corresponding to the line, plane normal, and glide directions, respectively, with dimensions $L_z = 19.9$ nm (80b), $L_y = 24.3$ nm, and $L_x = 58.7$ nm. This configuration contains in excess of 2.4 million atoms, which results in nominal strain rates of $1.7 \times 10^{6\sim7}$ s^{-1} for velocities between 10 and 100 m·s^{-1}. Figure 2 shows a schematic diagram of the computational box employed. The simulations were run on massively-parallel platforms ($>$500 processors) at Virginia Tech and Lawrence Livermore National Laboratory. The approximate computational cost of the simulations was 3.5×10^{-5} seconds per time step per atom.

3. Results.

3.1. Raw MD data.

The simulations are run for relatively long times to overcome any transients and develop statistically-meaningful behavior. Configuration data were extracted every picosecond regardless of the applied stress and the temperature. At 300 and 500K, each configuration is quenched *off-line* only for a few time steps to eliminate the thermal noise and facilitate the identification of the dislocation core. This is done using the centrosymmetry deviation parameter analysis employed in many other studies. From the position of the core, velocities are extracted as the derivative of the displacement-time curves for each case. The processed output of the simulations at 300K is shown in Fig. 3. Results for all the other temperatures are qualitatively identical. At each temperature, the stress is applied in roughly 50 MPa intervals from zero to the point of 'shear melting'. This phenomenon occurs when the screw dislocation moves too fast for the local heat generated on the glide plane to dissipate. Under such conditions, successive reentries through the periodic boundary heat the atomic layers around the glide plane above the melting point of the crystal. This causes the material to literally flow along the glide plane, locally removing any notion of crystallinity and dislocation structure. This is the case for the black curve in Fig. 3, corresponding to an applied stress of 1150 MPa. In addition, the threshold stress for dislocation motion within MD timescales, which we term σ_0, is measured (194 MPa in Fig. 3 for the 300K case). σ_0 is defined as the stress at which the dislocation moves within the first 100 ps, and is therefore an upper bound on the true threshold stress, imposed by the short MD timescales.

The velocities are measured from the slope of linear fits to the displacement-time curves at each (T, σ) condition. As mentioned earlier, the fits are only carried out after the finite-size reflections have subsided and the dislocations move in a smooth manner. By way of example, in Fig. 3 we show the fit for the 630-MPa simulation, which yields a velocity of 244 m·s^{-1}. The velocities obtained in this fashion are plotted in Figure 4 for the four temperatures considered in this study: 100, 200, 300, and 500K. Hereon, we refer
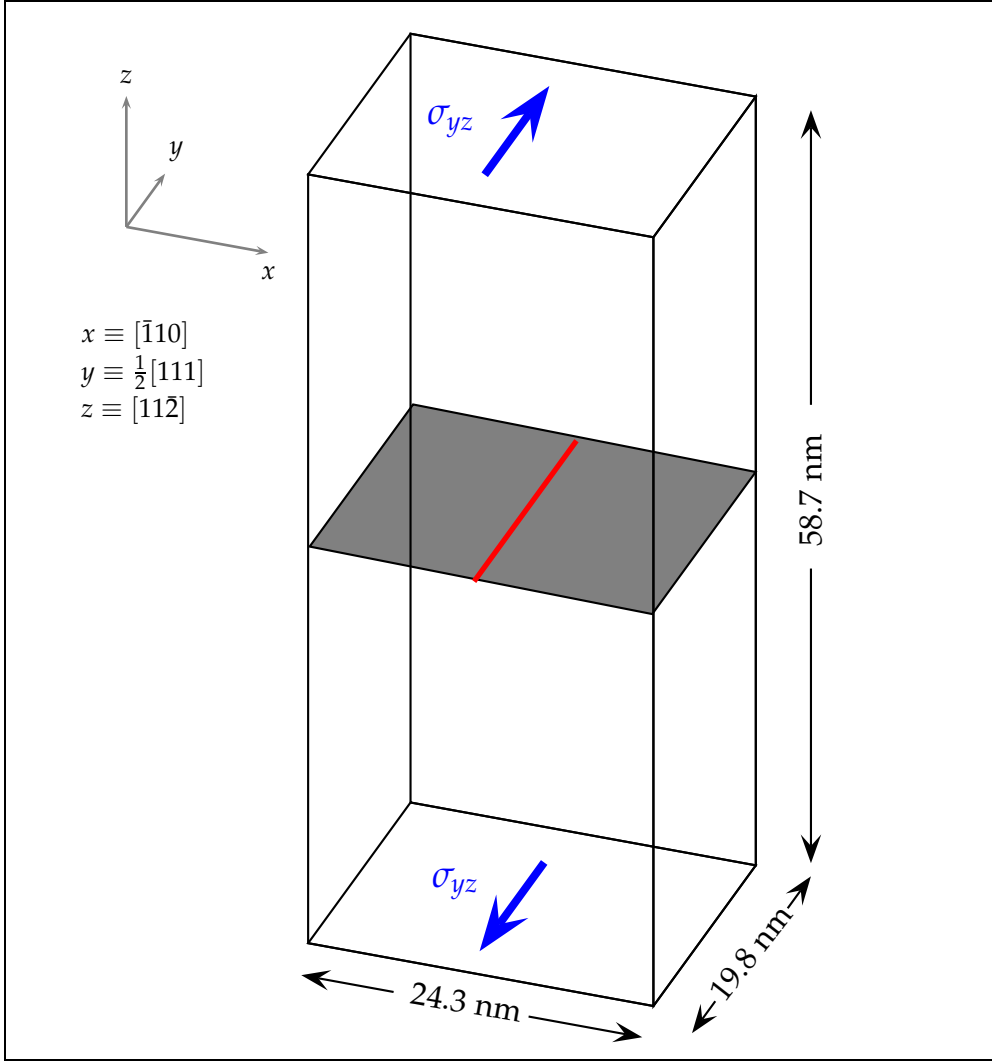
6

Figure 2: The simulation set-up used to measure the velocity response of a $\frac{1}{2}\langle 111 \rangle$ screw dislocation to applied stress at finite temperature. The shaded plane corresponds to the dislocation glide plane.

to the applied stress generically as σ, noting that the actual stress that the dislocation suffers may not be exactly identical to σ in view of the finite size effects described in Section 2.2.

Two regimes can be visually identified in Fig. 4, more ostensibly at lower temperatures. Initially, at low applied stresses, an exponential regime is clearly recognized, while at higher stresses the behavior is clearly linear. The dynamic transition is sharp at 100 and 200K, but becomes considerably more blurred at 300K, and particularly so at 500K. The inset to the figure shows the same data points on a logarithmic scale in an attempt to facilitate the identification of the dynamic transition, which is seen to occur at decreasing stresses with increasing temperature. These transition stresses are denoted by σ^*. Mathematically, σ^* is computed as the inflection stress, *i.e.* that at which the $v(\sigma)$ function transitions from convex to concave (in other words, when the local derivative of the v-σ curve starts to decrease). At 500K, this occurs over a stress range, more than at a specific value, but, acknowledging this ambiguity in the definition, here we
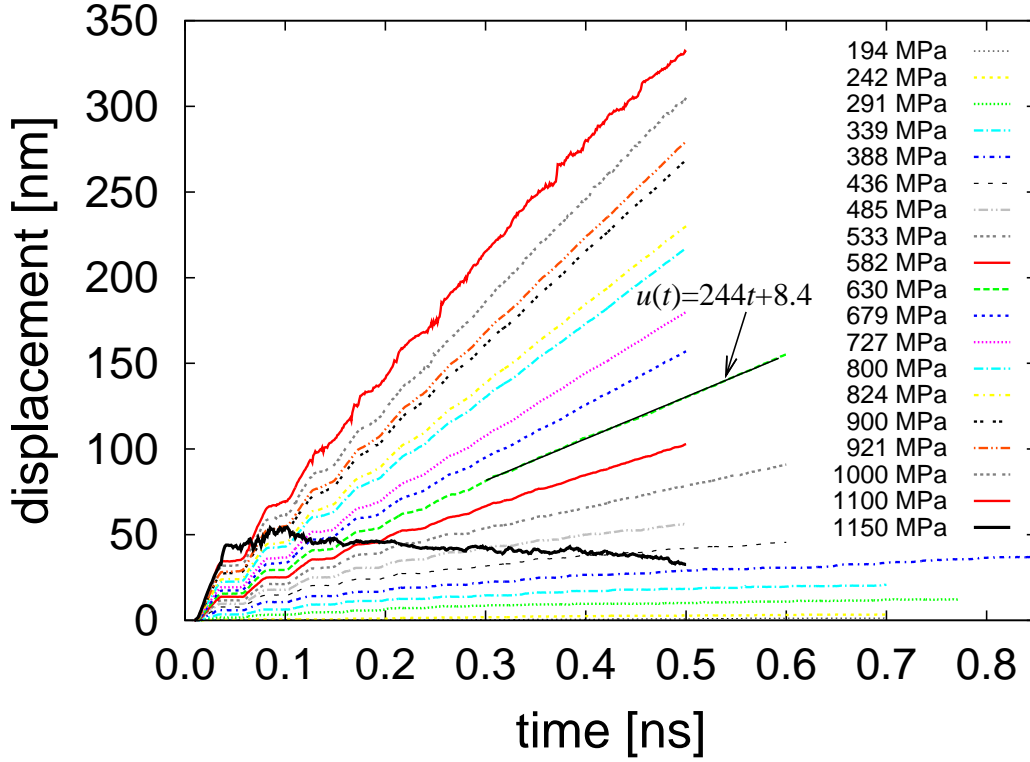
Figure 3: Dislocation displacement vs. time at 300K for all stresses considered here. The curves display an initial serrated behavior, follow by a steady state characterized by smooth glide. A linear fit to the smooth section of the 630-MPa curve is shown, yielding a velocity of 244 m·s^{-1}.

have taken $\sigma^*(500\text{K})$ as the first value in that stress range. The values of σ_0 and σ^* are given in Table 1 and plotted in Fig. 5 as a function of temperature.

Table 1: Calculated values of all temperature-dependent coefficients.

Temperature [K]		100	200	300	500
Threshold stress [MPa]	σ_0	650	400	194	104
Transition stress [MPa]	σ^*	797	770	633	312
Friction coefficient [$\times 10^{-4}$ Pa·s]	$\mathcal{B}$	2.5	2.4	2.7	2.9
Transition velocity [m·s^{-1}]	v^*	419	515	324	167

The exponential regime corresponds to the thermally activated mechanism of motion governed by KP nucleation, whereas the linear regime is the manifestation of some type of viscous motion. It is unclear if this corresponds to the classic phonon drag mechanism, as its onset occurs at stresses $< \sigma_P$, although, due to the displayed linearity, the theoretical treatment will be applied as if it was. In this context, $\sigma_*(T)$ has the meaning of a temperature-dependent transition stress, above which the *free* energy landscape is flat and the dislocation does not need to overcome any *effective* energy barrier. This is akin to the Peierls stress at 0K, which is approximately 1200 MPa for the potential employed here. We shall come back to
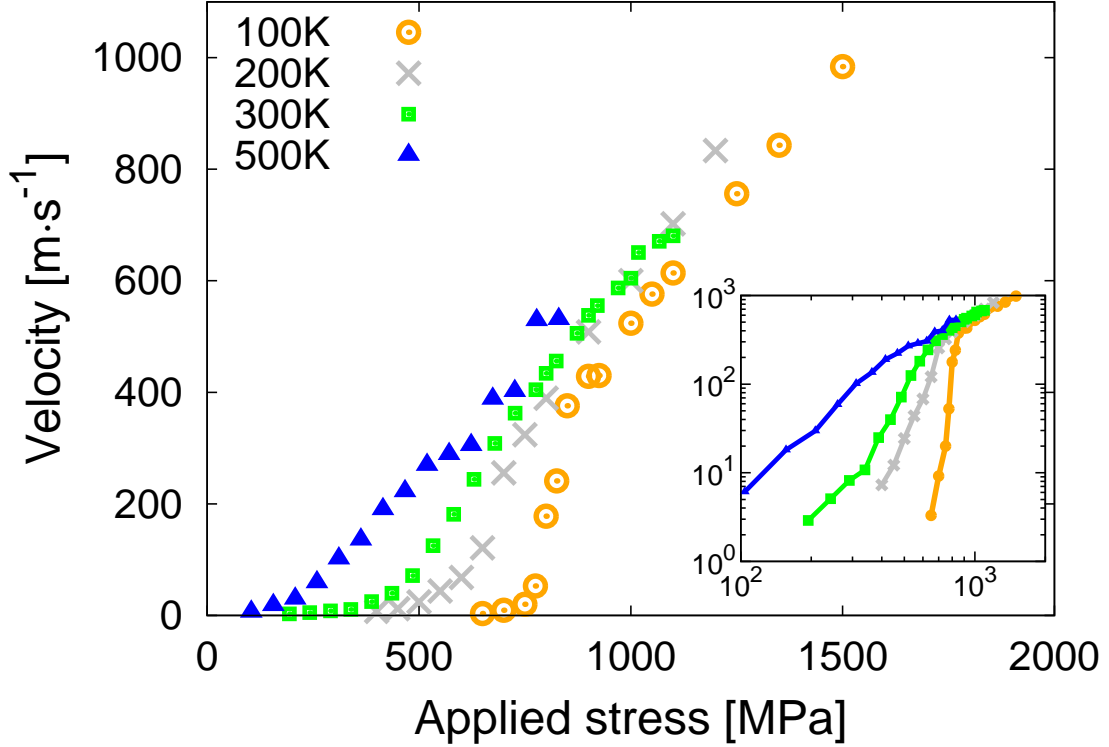
8

Figure 4: Dislocation velocities against applied stresses for all the temperatures considered here. The inset shows the same data in logarithmic scale, which allows for a better identification of the dynamic transition.

these issues in Section 4.

3.2. Mechanism of motion

Next, we describe some aspects of the mechanism of motion for $\sigma < \sigma^*$. Several workers have demonstrated the kink-pair mechanism in 3D dynamic simulations of $\frac{1}{2}\langle 111 \rangle$ screw dislocation motion for the Mendelev potential [30, 18], and we do not discuss it further here. Rather, we focus on the relationship between KP nucleation and glide plane.

As pointed out earlier, in conditions where a {112} plane is the MRSS plane, the two {110} planes bordering it at $\pm 30°$ are equally stressed with a Schmid factor of $\sqrt{3}/2$. At the same time, the elastic energy of a KP can be written as [36]:

$$H_0(h, w) = \frac{\mu b^2}{2\pi} \left[h \left(\frac{1}{1-\nu} \log \frac{h}{\rho} - 1 \right) - \frac{h^2 (1+\nu)}{4w (1-\nu)} \right] \tag{4}$$

where h and w are the kink's height and width and $w \gg h$ is assumed. ν and μ are Poisson's ratio and the shear modulus, respectively, and ρ is the elastic cutoff. With $w \gg h$ and $h \approx \rho$, the only non-negligible term in eq. 4 is that which is linear in $h^{\ddagger}$. Then, assuming a variation of H_{KP} with stress

---

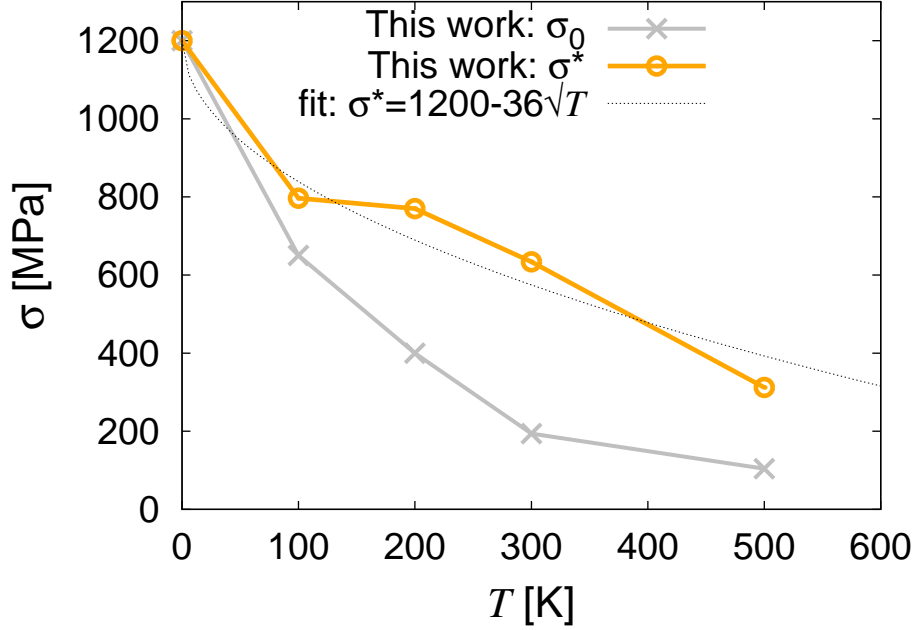$^{\ddagger}h^{\{110\}}/h^{\{112\}} = 1/\sqrt{3}$.

9

Figure 5: Evolution of the transition and threshold stresses with temperature. Also shown is the fit proposed by Wen and Ngan for σ^* [16], which provides very reasonable agreement with the MD data.

according to eq. 3, and $\sigma_P{}^{\{110\}}$ and $\sigma_P{}^{\{112\}}$ equal to, respectively, 1200 and 1300 MPa [30], we have $H_{\text{KP}}{}^{\{110\}} \lesssim 0.58 H_{\text{KP}}^{\{112\}}$, *i.e.* kink pairs on the adjacent $\{110\}$ planes are still more energetically favorable than their $\{112\}$ counterparts. Again, when coupled with the repulsive image forces discussed in Section 2.2, this picture favors alternating jumps between both $\{110\}$ planes in our simulation setup.

As a consequence, at low stress and temperature, $\{112\}$ glide is only *effective*, *i.e.* the overall glide plane observed from length scales far above the atomistic one is $\{112\}$, while it actually occurs by a succession of $\{110\}$ slip events observable only at the atomic level. At higher temperatures and stresses, one could expect significant deviations from this alternating slip mechanism as thermal fluctuations smear the (repulsive) effect of the traction boundaries. However, in analyzing the dislocation core carefully, we have seen that it undergoes a structural transformation from compact to dissociated between 350 and 400K, as clearly illustrated in Figure 6. This radically changes the available transition pathways for screw dislocation motion, as the dislocation can now only proceed in a manner consistent with pencil glide [16]. The combination of reduced transition paths and Peach-Köhler force direction prompt the dislocation to again follow an effective $\{112\}$ glide plane.

The mechanisms of motion described here are in disagreement with the interpretation by some workers that, under certain conditions, slip takes place by KP production directly on $\{112\}$ planes [45, 3].
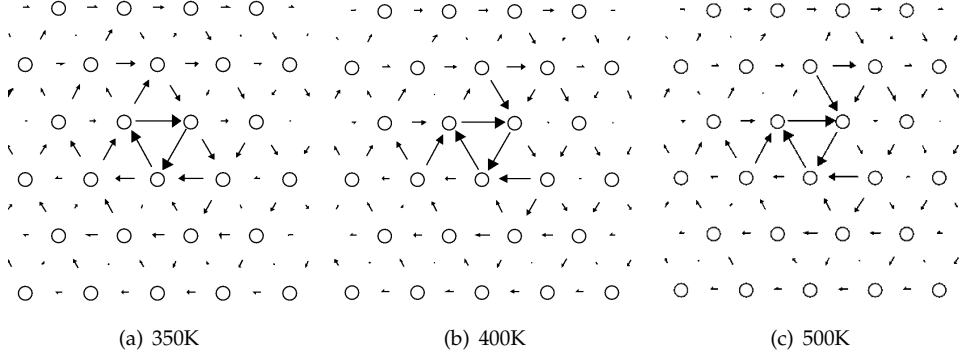
10

(a) 350K   (b) 400K   (c) 500K

Figure 6: Screw dislocation core structure at finite temperature illustrated using differential displacement maps [44]. The core suffers a transformation from compact to dissociated between 350 and 400K. Core configurations have been obtained by averaging the atomic positions over 1 ps.

3.3. Mobility functions

3.3.1. Thermally activated regime.

Within the kink-diffusion model, the velocity of a screw dislocation in the thermally-activated kink nucleation regime can be written as [38]:

$$v_{th} = hXJ_k, \tag{5}$$

where X, and J_k are defined as in Section 2.1. Replacing X with eq. 1 in eq. 5:

$$v_{th} = 2h\sqrt{J_k v_k},$$

and inserting eq. 2:

$$v_{th} = \frac{2hv_k}{a} \exp\left(-\frac{F_{\mathrm{KP}}(\sigma)}{2kT}\right), \tag{6}$$

where a is the kink translational distance, v_k is the kink velocity, and F_{KP} is the stress dependent free-energy of a KP. If one further assumes that the kink velocity follows Einstein's kinetic relationship:

$$v_k = \frac{2D_k}{a} \sinh\left(\frac{\sigma bha}{2kT}\right),$$

and that the mechanical work $\sigma bha \ll 2kT$, then:

$$v_k \approx D_k \frac{\sigma bh}{kT}, \tag{7}$$

where D_k is the kink diffusivity. Equation 6 then becomes:

$$v_{th} = 2D_k \frac{\sigma bh^2}{akT} \exp\left(-\frac{F_{\mathrm{KP}}(\sigma)}{2kT}\right) \tag{8}$$

Experimental studies have have shown that the formation entropy S_{KP} is only a small fraction of the total free energy [39]. This is substantiated by recent atomistic calculations of the vibrational entropy of finite screw dislocation segments [40]. Equation 8 can be written as:

$$v_{th} = 2D_k \frac{\sigma bh^2}{akT} \exp\left(-\frac{H_{\mathrm{KP}}(\sigma)}{2kT}\right).$$

11

For its part, the kink diffusivity is typically written as $D_k = \nu_0 a^2 \exp\left(-W_m/kT\right)$, where ν_0 is an attempt frequency and W_m is the kink migration energy. It is commonplace to assume $kT \gtrsim W_m$ on the basis that 'edge' type segments such as kinks undergo little or no lattice friction, so that their mobility is controlled by phonon scattering. However, kinks in α-Fe are known to have non-negligible widths, of the order of $6b$ [15] to $20b$ [17], which could result in significants deviations from pure edge character, and, thus, here we leave the explicit dependence on D_k.

When the kink pair expansion is limited by a finite line length L, the above expression needs to be corrected by a factor $\frac{L}{L+X}$. However, owing to the geometry constrains imposed in Section 2.1, it is reasonable to assume $X \approx L$ so that:

$$v_{th} = \frac{\sigma b h^2 \nu_0 a}{kT} \exp\left(-\frac{H_{KP}(\sigma)}{2kT}\right) \tag{9}$$

where we have further assumed that $W_m \ll H_{KP}/2$. For the stress dependence of H_{KP} we again use eq. 3. In principle, $p = 0.5$ and $q = 1.25$ can be fixed to the values predicted by linear elasticity theory. However, in a periodic box the activated state becomes distorted by the periodic image interactions (in the low stress limit) or by kink spreading (in the limit of stress approaching Peierls threshold). Therefore, we leave p and q as fitting parameters to be obtained from the MD data.

Equations 9 and 3 form a closed functional mobility law for screw dislocations for thermally activated motion. Next, the objective is to devise a global fitting procedure that retains only the stress and temperature dependence, *i.e.* a universal mobility function that can be used in the entire T and σ range. To this end, we first reduce the explicit stress dependence in eqs. 9 and 3 for numerical convenience to a non-dimensional form described by $s(T) = \sigma/\sigma^*(T)$. Additionally, we condense all the physical parameters in eqs. 9 into a single fitting constant A. The reduced expression is:

$$v_{th} = A\beta s \exp\left(-0.5\beta H_0 \left(1 - s^p\right)^q\right) \tag{10}$$

where $\beta = (kT)^{-1}$ is the reciprocal temperature. In eq. 10, we fix $H_0 = 0.65$ eV, which is the value obtained by molecular statics for the potential employed here [17]. Experimental estimates for H_0 from stress relaxation measurements in Fe give values in the 0.8~1.0 eV range [41, 42, 43, 45]. At this point, eq. 3 needs to be modified to account for the fact that, although here we are concerned with $\frac{1}{2}\langle 111\rangle\{112\}$ mobilities, eq. 3 refers to kink pair formation on $\{110\}$ planes. As shown in Section 3.2, glide on the $(11\bar{2})$ plane proceeds via successive nucleation of KP on alternate $(01\bar{1})$ and $(10\bar{1})$ planes forming $30°$ with the MRSS plane. The Schmid factor on these two planes is $\sqrt{3}/2$ and, therefore, s must be multiplied by it to ensure that the correct stress for KP formation and propagation is considered.

Using eq. 10 and the transition stresses in Table 1, we perform a collective least-squares fit to the data in Fig. 4 and obtain values of: $A = 7.4 \pm 0.6$ eV·m·s^{-1}, $p = 1.1 \pm 0.2$, and $q = 1.99 \pm 0.2$. As Fig. 7 shows, the resulting mobility function provides a very good fit for the velocities corresponding to the thermally activated regime, particularly at 100 and 200K. The overall fitting error is approximately 5%. It is worth mentioning that we have also performed a fit using the thermally activated mobility law used by Naamane *et al.* [46], which does account for both forward and backward jumps and assumes $p = 0.5$ and $q = 1$. Nevertheless, the resulting fit provides slightly worse agreement with the MD data than the primary one used here. The mobility function in numerical form is thus:

$$v_{th}(s, \beta) = 7.4\beta s \exp\left\{-0.32\beta \left(1 - 0.85s^{1.1}\right)^2\right\}.$$

12

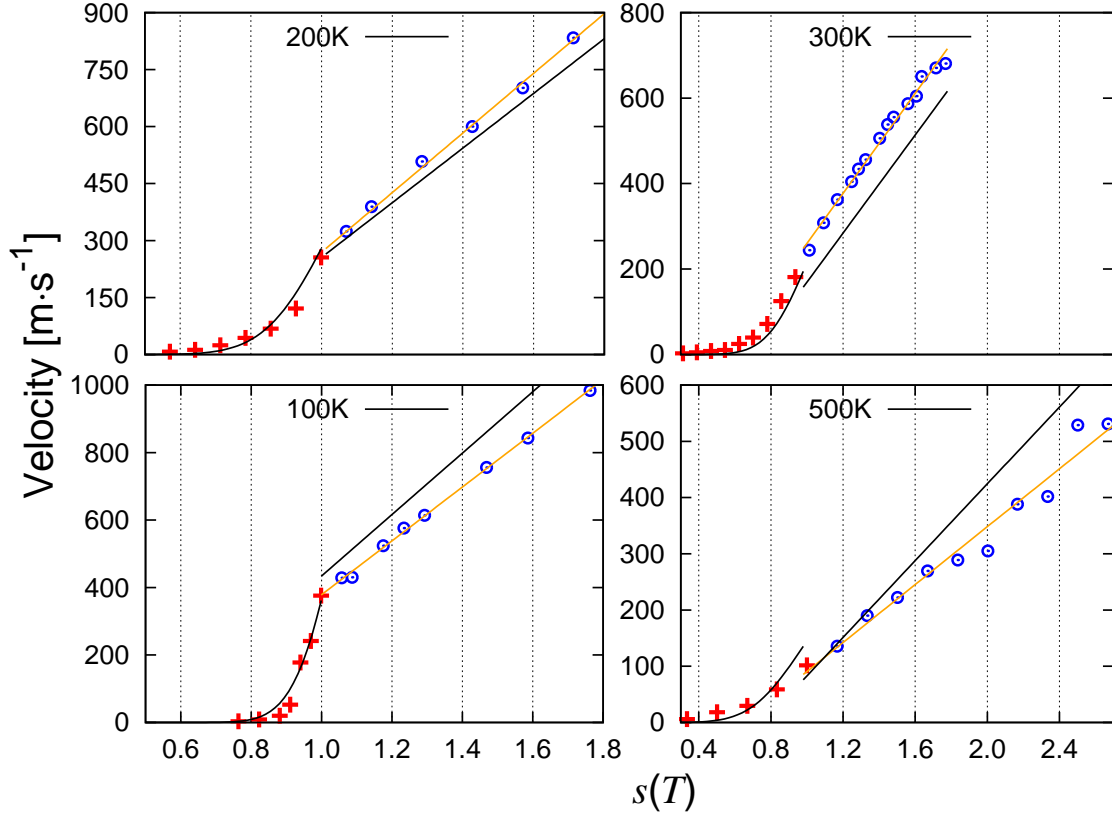To fully close the mobility law, one must provide the temperature dependence of σ^* through some

Figure 7: Comparison between the fitted mobility laws and the MD data at each temperature. We note that the mobility is not continuous at σ^*, and that an appropriate 'stitching' between the mobilities in each regime must be performed prior to their use in DD simulations. The orange lines represent the individual fits according to eq. 14.

suitable analytical law. Following Ngan and Wen [34], the relation between σ^* and T can be described by:

$$T \propto \left(1 - \frac{\sigma^*}{\sigma_P}\right)^2,$$

where we have made use of the equivalence between activation energy and temperature at constant strain rate proposed experimentally (*e.g.* $H/kT \approx 27$ at 1.7×10^{-4} s^{-1} [47]). Then we fit the σ^*-T data points in Table 1 to a law of the type:

$$\sigma^* = \sigma_P - C\sqrt{T} \tag{11}$$

The fit, which yields a value of $C = 36.1 \pm 2.4$ MPa·K$^{-1/2}$, is also shown in Fig. 5. Incidentally, the above expression predicts a value of $\approx$1100K as the temperature at which the transition stress vanishes. The final mobility function in the thermally activated regime is then:

$$s = \frac{\sigma}{1200 - 36\sqrt{T}}$$

$$v_{th}(s, \beta) = 7.4\beta s \exp\left\{-0.32\beta\left(1 - 0.85s^{1.1}\right)^2\right\} \tag{12}$$

13

which gives the screw dislocation velocity for each (σ, T) pair.

3.3.2. Linear regime.

At shear stresses above σ^*, the dislocations clearly transition into a linear velocity regime governed by some kind of viscous motion. In principle, one could use a universal fitting function of the type:

$$v_l(T) = ds + e \tag{13}$$

where d and e are also temperature-dependent constants. d is inversely proportional to the friction coefficient $\mathcal{B}$ and thus should scale with temperature as $\sim T^{-1}$. For its part, e should be related to the velocity corresponding to σ^*, *i.e.* the *transition* velocity v^*. However, because we have no *a priori* information about the temperature dependence of these constants, we first fit each linear mobility data set in Fig. 4 individually using the standard viscous law:

$$v_l = \frac{\sigma b}{\mathcal{B}(T)} - v^*(T), \tag{14}$$

In this fashion, we compute $\mathcal{B}$ and v^* for each T to gain insights into their temperature dependence. The results of the fit are shown in Fig. 7 as orange lines. The values for $\mathcal{B}$ and v^* are given in Table 1. As the data show, $\mathcal{B}$ displays virtually no temperature dependence, while that of the transition velocities is not clear at first glance. In searching for a suitable temperature dependence for v^*, we note that v^* is zero both when $\sigma^* = 0$ and when $\sigma^* = \sigma_P$. This is because those are the two instances when there is no longer need for thermally-activated KP nucleation to attain dislocation motion. In terms of temperature, these two limits correspond, respectively, to the temperature at which the dislocation free energy is equal to the Peierls barrier (not precisely known from the simulations, but estimated from eq. 11 at approximately 1100K), and 0K. v^* is plotted as a function of σ^* and T in Figure 8, where the temperature scale follows eq. 11. To ensure $v^*(\sigma^* = 0) = 0$, we fit the data shown in the figure to a third-degree polynomial of the type:

$$v^* = \sigma^* \left(c_2 \sigma^{*2} + c_1 \sigma^* + c_0 \right),$$

which results in $c_0 = -4.4 \times 10^{-2}$, $c_1 = 2.2 \times 10^{-2}$, and $c_2 = -1.8 \times 10^{-6}$ (we omit the units of the fitting constants for clarity). The fitted polynomial is also shown in Fig. 8. The dependence with temperature is trivially obtained by substituting $\sigma^* = 1200 - 36\sqrt{T}$ into the fitted polynomial:

$$v^*(T) = 0.079T\sqrt{T} - 5.456T + 93.9\sqrt{T} + 3.5 \tag{15}$$

where the sensibility of the fit to the number of significant figures taken for each coefficient is noted.

With the functional dependencies established above, we are now in a position to expand eqs. 13 and 14 into a mobility law for the linear regime:

$$v_l(s, T) = as + bs\sqrt{T} - 0.079T\sqrt{T} + 5.456T - 93.9\sqrt{T} - 3.5$$

Fitting to the data given in Fig. 4 for all temperatures yields values of $a = 1370 \pm 36$ and $b = -46 \pm 2$. From the value of $a = \sigma_P b/\mathcal{B}$, an average $\mathcal{B} \approx 2.2 \times 10^{-4}$ Pa·s can be extracted, in good agreement with the tabulated values for the individual fits given in Table 1. The final mobility function in the linear regime is therefore:

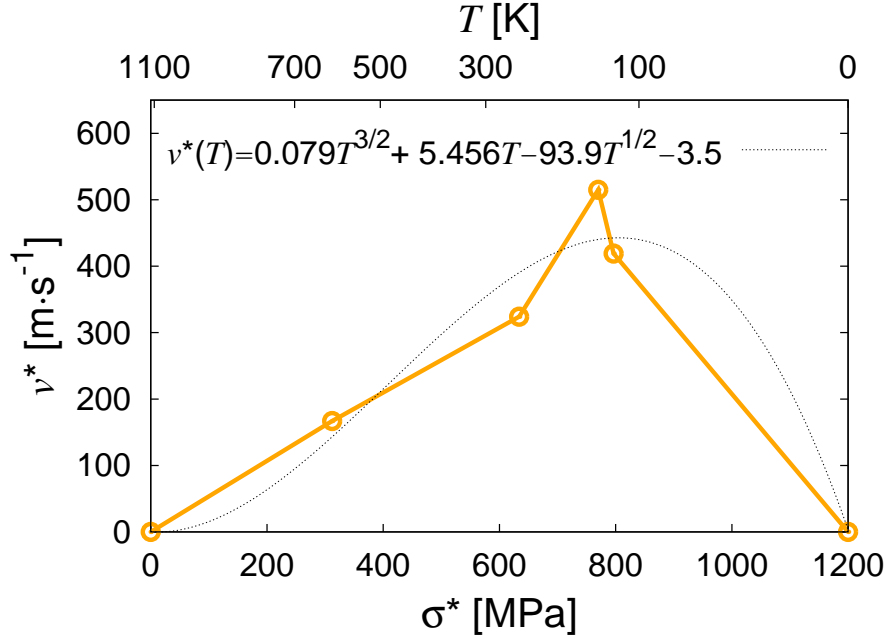$$v_l(s, T) = 1370s - 46s\sqrt{T} - 0.079T\sqrt{T} + 5.456T - 93.9\sqrt{T} - 3.5 \tag{16}$$

14

Figure 8: Relationship between the transition velocity v^* and σ^* and T.

The results of this fit are also shown in Fig. 7.

Thus, a closed-form mobility function for $\frac{1}{2}\langle 111 \rangle$ screw dislocations in α-Fe gliding on $\{112\}$ planes in the twinning sense as a function of stress and temperature is proposed based on MD simulations:

$$v(s, T) = \begin{cases} 8.6 \times 10^5 s T^{-1} \exp\left\{ -3.8 \times 10^3 T^{-1} \left(1 - 0.85 s^{1.1}\right)^2 \right\}, \text{ for } s \leq 1 \\ 1370s - 46s\sqrt{T} - 0.079T\sqrt{T} + 5.456T - 93.9\sqrt{T} - 3.5, \text{ for } s > 1 \end{cases} \tag{17}$$

where $s = \frac{\sigma}{1200 - 36\sqrt{T}}$.

4. Discussion and conclusions

In this paper, we have carried out simulations of $\frac{1}{2}\langle 111 \rangle (11\bar{2})$ screw dislocation motion as a function of stress and temperature in order to fit functional mobility laws to be used in mesoscale methods. Below we discuss several aspects related to the validity of our approach and the applicability of the mobility functions proposed.

Let us start by discussing the validity of MD simulations for this task, *vis a vis* the high attendant strain rates. Dislocation motion simulations can be run prescribing the strain rate [13] or, alternatively, the applied stress [26, 30]. If one chooses the former, the velocity of the dislocation is also prescribed, and the corresponding stress is extracted as the output of the simulations. Because the strain rates for dislocations to have a noticeable motion within MD time scales have to be exceedingly high, it is difficult to argue against the statement that MD strain rates are often excessively above realistic experimental ones. However, if one performs stress-controlled simulations, it is the velocity that is the output, not the strain rate. Velocities are related to the strain rate trough Orowan's equation ($\dot{\varepsilon} = \rho_d vb$, where ρ_d is the dislocation density). However, for a fixed dislocation line length, one can obtain converged mobilities

15

above a certain box size. What this means is that the measured velocity does not change even if the box
dimensions (except the line length) are increased arbitrarily, *i..e* ρ_d is decreased arbitrarily. Then, the only
certainty is the σ-v correspondence, which is, following this argument, independent of the strain rate.

Next, the adequacy of the fitting functions given in eq. 17 is discussed. Equation 10, describes the
relation between v and σ and T in the thermally activated regime. The functional form for H_{KP}, eq.
3, although phenomenological in nature, is known to provide a good linkage between H_0 and zero as a
function of the applied shear stress, and has been widely used in the literature [19, 31, 32]. The exponents p
and q obtained here are somewhat larger than the expected values predicted by linear elasticity, and other
calculations. However, the validity of our fit is best assessed by comparing against existing experimental
measurements and atomistic calculations. To remove the dependence on the quantitative differences
between experiments and atomistics, on the one hand, and different interatomic potentials, on the other,
of the Peierls stress and KP Nucleation energy, we compare in Figure 9 the ratio H_{KP}/H_0 obtained as
function of σ/σ_P from several sources. The figure includes experimental data from Aono *et al.* [47] and
Quesnel *et al.* [48] and atomistic results obtained here and from Wen and Ngan [16]. As shown, our
fit with $p=1.1$ and $q=2$ provides excellent agreement both with experimental data and our own static
calculations. In particular, the good agreement between the MD and static calculations performed in this
work is encouraging in light of all the assumptions that enter eq. 10.
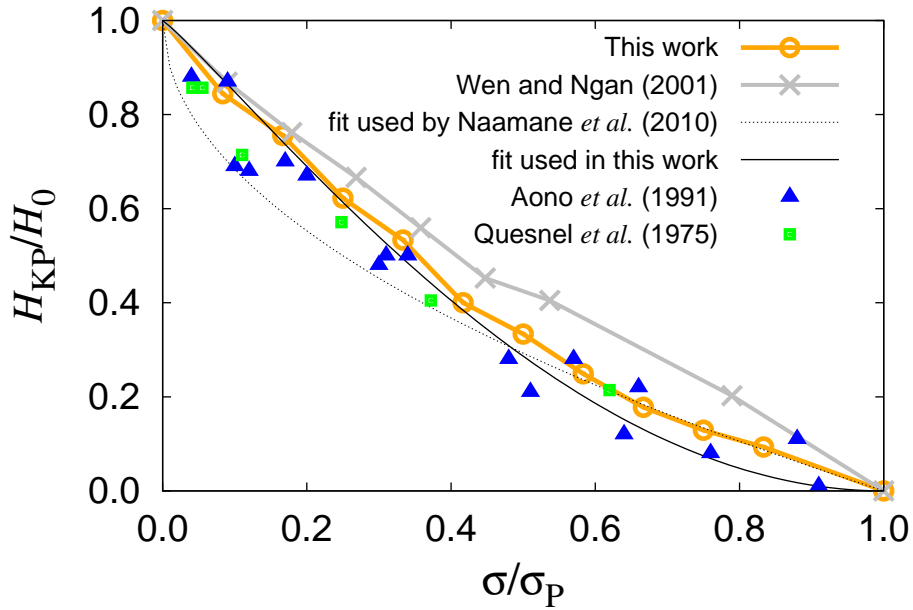

Figure 9: Variation of the normalized KP formation energy with normalized stress. Data from two molecular statics calculations are shown: our own, and Wen and Ngan's [16]. Experimental data points by Aono *et al.* [47] and Quesnel *et al.* [48] are also shown for comparison. The fit obtained in this work, with $p=1.1$ and $q=2$, and that used by Naamane *et al.* [46], with $p=0.5$ and $q=1$, are given.

For the linear regime of motion, some *ad hoc* assumptions have been made. First, we have neglected
any temperature dependence of the viscous drag coefficient $\mathcal{B}$. This was established on the basis of
independent linear fits to the MD values, which revealed no discernible temperature dependence. Second,

we have assumed a polynomial form for the variation of the transition velocity v^* with temperature, although a physical justification for the temperatures (stresses) at which v^* should vanish does exist. Even though the third-degree polynomial used was chosen for numerical convenience, it manages to provide a reasonable fit to the data given in Fig. 8, as also seen in Fig. 7. The highest discrepancy is observed for the simulations at 500K, which is precisely the temperature at which $\mathcal{B}$ is highest (cf. Table 1) and most different from the average value extracted from eq. 16.

Next, let us analyze the issues associated with {112} glide. As was stated in Section 1, slip in bcc materials is known to proceed principally on {110} planes. However, while, at low temperatures and stresses, the potential used in this work predicts screw dislocation glide on {110} planes [30], we have shown that above 350K the dislocation core loses its compact structure and adopts a more extended structure. This has two immediate effects: first, the transition stress decreases; and second, the dislocation then glides on multiple slip planes in the twinning zone (akin to the so-called 'pencil glide'). This mechanism notwithstanding, slip proceeds always by way of elementary {110} episodes of KP formation, regardless of what the *effective* glide plane is seen to be. This is why, when properly constrained, the dislocation can be made to make successive jumps on the two {110} planes adjacent 30° above and below to a twinning {112} plane so as to appear to glide on that {112} plane. These are precisely the conditions under which this study has been carried out.

Because of the above argument, the critical and transition stresses measured here pertain to KP formation on {110} planes and can be compared directly with other calculations and experimental data associated with {110} slip. Figure 10 shows the temperature dependence of the critical glide stress, σ_0, obtained here compared to the dynamic data obtained by Domain and Monnet [13], and the static results of Wen and Ngan (using a different interatomic potential) expressed in kT space [16]. In addition, experimental data from Kuramoto *et al.* [5] and Brunner and Diehl [6] are also shown. Both of these experiments were carried out under conditions that favor glide on {110} planes at strain rates $< 10^{-4}\,\mathrm{s}^{-1}$. As in Fig. 9, to remove the effect of the discrepancy observed in σ_P between experiments and atomistic simulations, we plot the ratio σ/σ_P as a function of temperature. As the figure demonstrates the agreement for $T < 300$K between our data and both experiments and atomistic calculation is excellent. However, at higher temperatures, the MD calculations deviate from the static values in that they appear to saturate or decline more slowly to their zero value. Future studies will determine the temperature at which the threshold stress vanishes for the Mendelev potential.

Of course, the ultimate objective of works such as the present one is to generate mobility laws that can be elevated to higher temporal and spatial scales by being integrated into models of higher statistical level, *e.g.* dislocation dynamics, phase field, etc. In this sense, we note that our work, which provides mobilities for a given slip system, is only one step in such a direction, and that more calculations on other slip systems, perhaps using other interatomic models, must be carried out before a full mobility law can be produced. In any case, our simulations provide non-linear laws that represent an improvement over uniform, character-independent variants (known as 'BCC0') used in several studies [49]. Other workers have used non-linear expressions similar to eq. 9 that are typically fitted to experimental data or molecular statics calculations [19, 20, 46], *i.e.* not obtained in a self-consistent fashion as in this paper[§]. In any case,

---

[§]This is not to say that they are not satisfactory, in several regards they might be better suited for DD calculations than the ones presented here.
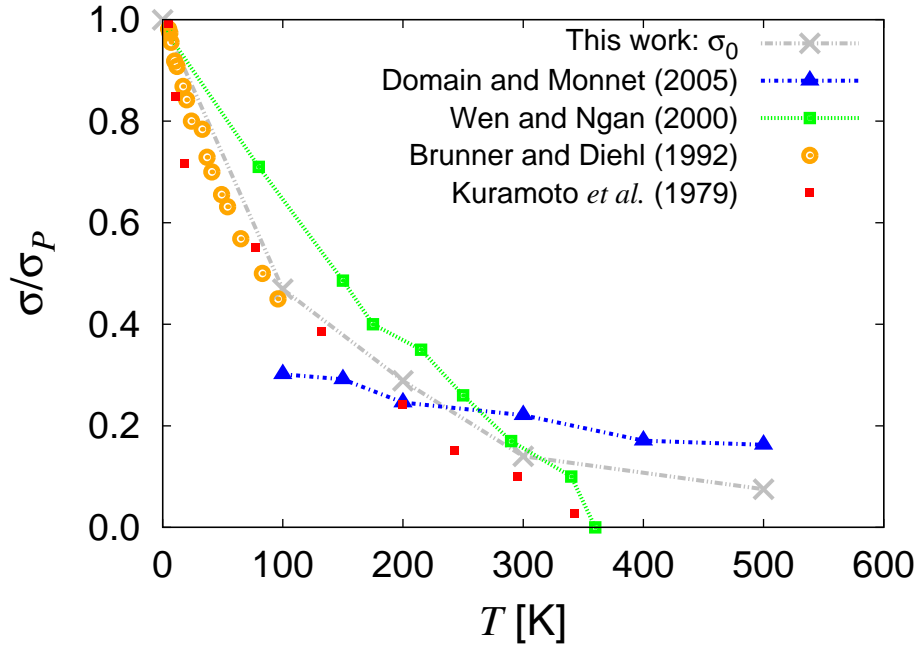
Figure 10: Comparison of the normalized threshold stress obtained in this work to atomistic results [16, 13] and the experimental values of the flow stress in pure single Fe crystals measured by Kuramoto *et al.* [5] and Brunner and Diehl [6]. The normalization factors for the experimental data were 363 [46] and 380 MPa, respectively.

a unified mobility function, apt for use in DD, must be continuous and differentiable in the entire stress and temperature ranges. Thus, the numerical usefulness of eq. 17 for dislocation dynamics calculations hinges on an appropriate 'stitching' of the thermal and linear mobilities presented here. This can be achieved using suitable splines or via harmonic averaging [50]. However, this belongs to the realm of functional analysis and is not elaborated on further. With regard to range of applicability of eq. 17, the very definition of s imposes a limit of T=1100K for our mobility function. Evidently we stand by our explored temperature interval of $100 < T < 500$K, but it is unclear if the functions supplied here are valid beyond it. It is important to emphasize that v_l in eq. 16 is only meaningful for $s > 1$.

Acknowledgments.

References

[1] R R. Kossowsky and N. Brown, *Acta Metall.* **14** (1966) 131.

18

370 [2] W. Wasserbäch, *Phil. Mag.* A **53** (1986) 335.

371 [3] D. Brunner and J. Diehl, *physica status solidi* (a) **124** (1991) 155.

372 [4] T. Suzuki, H. Koizumi, and H. O. K. Kirchner, *Acta Metall. Mater.* **43** (1995) 2177.

373 [5] E. Kuramoto, Y. Aono, and K. Kitajima, *Philosophical Magazine* A **39** (1979) 717.

374 [6] D. Brunner and J. Diehl, *Z. Metallkd.* **83** (1992) 828.

375 [7] T. J. Balk, K. J. Hemker, *Philosophical Magazine* A **81** (2001) 1507.

376 [8] M. J. Mills, N. L. Baluc, P. M. Sarosi, *Microscopy Research and Technique* **69** (2006) 317.

377 [9] D. Caillard, *Acta Materialia* **58** (2010) 3493.

378 [10] R. Chang, *Philosophical Magazine* **16** (1967) 1021.

379 [11] P. C. Gehlen, *Journal of Applied Physics* **41** (1970) 5165.

380 [12] T. Harry and D. J. Bacon, *Acta Materialia* **50** (2002) 195.

381 [13] C. Domain and G. Monnet, *Physical Review Letters* **95** (2005) 215506.

382 [14] L. Ventelon and F. Willaime, *Journal of Computer-Aided Materials Design* **14** (2007) 85.

383 [15] M. S. Duesbery, *Acta Metallurgica* **31** (1983) 1747.

384 [16] M. Wen and A. H. W. Ngan, *Acta Materialia* **48** (2000) 4255.

385 [17] L. Ventelon, F. Willaime, and P. Leyronnas, *Journal of Nuclear Materials* **386-388** (2009) 26.

386 [18] P. A. Gordon, T. Neeraj, Y. Li, and J. Li, *Modelling Simul. Mater. Sci. Eng.* **18** (2010) 085008.

387 [19] M. Tang, L. P. Kubin, and G. R. Canova, *Acta materialia* **46** (1998) 3221.

388 [20] J. Chaussidon, C. Robertson, D. Rodney, and M. Fivel, *Acta Materialia* **56** (2008) 5466.

389 [21] W. Cai and V. V. Bulatov, *Materials Science and Engineering* A **387-389** (2004) 277.

390 [22] "Handbook of Materials Modeling", ed. by S. Yip (Springer, The Netherlands, 2005).

391 [23] V. V. Bulatov and W. Cai, "Computer Simulations of Dislocations" (Oxford University Press, 2006).

392 [24] J. Chang, W. Cai, V. V. Bulatov, and S. Yip, *Materials Science and Engineering* A **309-310** (2001) 160.

393 [25] J. Marian and A. Caro, *Phys. Rev.* B **74** (2006) 024113.

394 [26] J. Marian, W. Cai, and V. V. Bulatov, *Nature Materials* **3** (2004) 158.

395 [27] S. J. Plimpton, *J. Comp. Phys.* **117** (1995) 1.

396 [28] M. I. Mendelev, S. Han, D. J. Srolovitz, G. J. Ackland, D. Y. Sun, and M. Asta, *Phil. Mag.* **83** (2003) 3977.

397 [29] S. L. Frederiksen and K. W. Jacobsen, *Philos. Mag.* **83** (2003) 365.

398 [30] J. Chaussidon, M. Fivel, and D. Rodney, *Acta Mater.* **54** (2006) 3407.

399 [31] D. Rodney and L. Proville, *Phys. Rev.* B **79** (2010) 094108.

400 [32] G. Monnet, C. Domain, S. Queyreau, S. Naamane, and B. Devincre, *Journal of Nuclear Materials* **394** (2009) 174.

401 [33] U. K. Kocks, A. S. Argon, and M. F. Asby, *Prog. Mater. Sci.* **19** (1975) 1.

402 [34] A. H. W. Ngan and M. Wen, *Computational Materials Science* **23** (2002) 139 .

403 [35] T. C. T. Ting and D. M. Barnett, *International Journal of Solids and Structures* **30** (1993) 313.

404 [36] H. Koizumi, H. O. K. Kirchner, and T. Suzuki, *Acta Metall. Mater.* **41** (1993) 3483.

405 [37] A. Seeger, *Zeitschrift für Metallkunde* **93** (2002) 760.

406 [38] J. P. Hirth and J. Lothe, "Theory of dislocations" (Wiley, New York, 1981).

407 [39] W. A. Spitzig and A. S. Keh, *Acta Metall.* **18** (1970) 1021.

408 [40] P. C. Schuck, J. Marian, J. B. Adams and B. Sadigh, *Philosophical Magazine* **89** (2009) 2861.

409 [41] W. A. Spitzig and A. S. Keh, *Acta Metall.* **18** (1970) 611.

410 [42] S. Takeuchi and K. Maeda, *Acta Metall.* **25** (1977) 1485.

411 [43] A. Seeger, *Materials Science & Engineering* A **319-321** (2001) 254.

412 [44] V. Vitek, *Cryst. Latt. Defects* **5** (1974) 1.

413 [45] A. Seeger and W. Wasserbäch,, *Phys. Stat. Sol.* (a) **189** (2002) 27.

414 [46] S. Naamane, G. Monnet, and B. Devincre, *International Journal of Plasticity* **26** (2010) 84.

415 [47] Y. Aono, E. Kuramoto and K. Kitajima, in: "Dislocation Dynamics and Plasticity" (Springer, Berlin, 1991) p. 94.

416 [48] D. J. Quesnel, A. Sato, and M. Meshii, *Mater. Sci. Eng.* **18** (1975) 199.

417 [49] A. Arsenlis and M. Tang, *Modelling and Simulation in Materials Science and Engineering* **11** (2003) 251.

418 [50] N. Barton, J. V. Bernier, R. Becker, A. Arsenlis, R. Cavallo, J. Marian, M. Rhee, H.-S. Park, B. A Remington, and R. T. Olson,
419   *Journal of APllied Physics* **109** (2011) in press.